

PERFORMANCE ENHANCEMENT FOR ROTARY AIR PREHEATER OF A THERMAL POWER PLANT

* Sinan Mazin Hazim¹

Dr. Mohammed H. Alhamdo²

1) Ministry of Electricity (GCEP), (former Ph.D. student in Mechanical Engineering Department, Mustansiriyah University, Baghdad, Iraq.

2) Prof., Mechanical Engineering Department, Mustansiriyah University, Baghdad, Iraq.

Received 8/3/2020

Accepted in revised form 21/6/2020

Published 1/11/2020

Abstract: The corrosion phenomenon is considered the main problems for air preheater in thermal power plant. The boiler flue gas contamination leads to decrease the air preheater performance and increases the maintenance cost, which causes the degradation of the cold end heating elements and thus leads to decrease the heat recovery rate. In this study, an experimental investigation was done for the transient thermal behavior and the pressure drop of the standard regenerative air preheater (P_{matrix}) model, evaluating the performance factor, then modifying the air preheater (P+CG) model by changing the plates at the cold end last basket to the coarse gravel media. Since the gravel media have low thermal conductivity and predicted to give a high pressure drop, a new technique was done for the modified air preheater to compensate the low heat transfer rates and reduce the pressure drop in the gravel media by inserting bypass tubes at ratios (i and s), Which, the (i) model represents the inner aperture of tubes for the hot baskets facing to the inner aperture of tubes for the cold basket. While (s) model the insertion the tubes of the hot baskets as a staggered distribution with the tubes for the cold basket. The experimental investigation was carried out for the Reynolds number based on the test duct hydraulic diameter at a range of $24500 < Re < 98000$ for each charge and discharge periods. The experimental results are presented in terms of the average heat transfer rate and the pumping power for matrix models. The experimental measured results corroborated that the bypass tubes have a significant

impact on improving the heat transfer rate and the pressure drop reduction of the modified air preheater matrix. The results showed that the best performance factor was achieved in the air preheater (P+CG+Ts) model which found to be in the range of 0.7-0.31 at high and low Reynolds. However, this improvement increased the pumping power by 13% than the (P_{matrix}) model.

Keywords: Air Preheater, Modified, Gravel media, the Bypass tube.

1. Introduction

Air-pre heaters is a regenerative heat exchanger, which is used in many applications, such as in the industrial furnaces and in the boilers of a power plant to raise the temperature for the supply of cold air before entering to the combustors by recovering the exhaust hot gases temperature. That leads to improved combustion to the furnaces and thus improves the boiler efficiency. The air preheater heating elements are subjected to the continually separately periodic modes, in the one mode, the flue gas is passing through the heating elements matrix of air preheater in one direction to absorb more heat as called a charge period, then the fresh

*Corresponding Author: sinan2004_5@yahoo.com

cold air passes through the heating elements matrix in a counter direction that is heated by the accumulated heat of the matrix as called a discharge period. Each mode has the same periodic time depending on the air preheater design of the elements rotating actual in power plant at (1-3 rpm) [1]. The flue gases caused many problems of air-preheater efficiency which decrease the heat transfer and the reliability of power plants. One of these problems is the flue gas ash particle that deposits and accumulated on the heating elements surface. The accumulated soot resulted in a decrease in heat transfer between the passing gases and the heating elements and caused the blockage. For this reason, a periodic cleaning medium such as soot blower by dry steam or air is provided to prevent the fouling. The other problems are Sulfuric acid dew corrosion stemming from the sulfur contained in the fuel oil that develops at the cold end zone of an air preheater which leads to breakdown of the metal plates and thus decreases the recovery heat rates [2]. Therefore, the cold end heating elements of the air preheater have to be more corrosion resistant to decrease both the corrosion rates and the maintenance cost. Typically, the materials used for the heating elements are carbon steel at the hot end and low-alloy corrosion-resistant steel (Corten steel) for the cold end [3]. A good heating elements material and design led to improving the thermal performance; which has been the subject of various studies. For instance, Ghodsipour and Sadrameli [4] estimated the maximum regenerator effectiveness as a function of rotational speed as well as charge and discharge streams flow, a mathematical model was solved and optimized with the experimental design method. Al-Kayiem and Mahdi, 2010 [5] studied experimentally the performance improvement of rotary air preheater for roughening the heating elements

by pin tabulator and compared with the standard heating elements. The results indicated that the roughness heating elements enhance the heat transfer and reach to the maximum at the pin pitch to pin height ratio = 10 for both charging and discharge periods. Vulloju et al., 2014 [6] conducted lab-scale experiments of air preheater to compare the two designs for the corrugated plate profile for better hydrodynamic. It was concluded that hydraulic diameter does not affect the performance between the two profiles, since the difference between the hydraulic diameters is small. Also, the fluid pumping power for the flat notched profile is less than for the double undulated profile. Heidari and Hajidavalloo, 2014 [7] modeled a full scale of the rotary air preheater using three-dimensional with treating the preheater matrix as a porous media. Many factors are tested, including the effect of changing matrix material for non-corrosive materials, it was concluded that the difference between the selective materials is not very significant compared with the standard material. Baba et al. 2016 [8] conducted a numerical investigation for a full-scale air preheater model to test the influence of the ambient temperature and seal the leakage on the air preheater performance at different load conditions. A three-dimensional model of rotary air preheater under unsteady state has been carried out by using ANSYS FLUENT. The results cleared that increasing the ambient temperature leads to an increase in the pressure drop for both the air and the flue gases, the increasing of the seal leakage leads to decreasing the efficiency of the boiler. Wang et al., 2017 [9] compared experimentally the flow and the heat transfer performance between the standard metal matrix of the air preheater and for the honeycomb ceramics matrix which have good corrosion resistance. It was concluded that the standard matrix gives a higher discharged outlet air temperature and less pressure drop

than the honeycomb matrix. In many studies, the thermal enhancement for the air preheater has been done by modifying all the matrix without considering the high cost of the air preheater. So, the study focused on enhancing a part of the air preheater matrix that gives the lowest heat transfer and supposed to the dew point corrosion. Besides that, few researchers have taken into account the transient effect for the heat transfer rate calculation of the air preheaters. So, the main objective of this study is to investigate the pressure drop and the transient heat transfer performance of the standard matrix air preheater (P_{matrix}) model, which has metal corrugated plates, and then compared with a modified air preheater matrix (P+CG) model by filling the last end part of the matrix by the gavel media instead of the plates. Many numbers of the by-pass tubes are inserted through the (P+CG) matrix in a proper technique, this is expected to provide more hot air to the gravel media at the charging mode and hence improve the heat transfer rate at the discharged mode. Besides that, the tubes lowering the high pressure drop for (P+CG) matrix result in an improve meant in the performance of the air preheater.

2. Experimental Section

The 90 cm long air preheater test section is placed in a vertical position for ease of changing the basket matrices. It consists of five frame baskets with dimensions of 50 cm width \times 50 cm length \times 17 cm height and is separated with 1.5 cm between each other. This characteristic length is based on a real design of an air-preheater installed in south Baghdad thermal power plant that was listed in the table (1). The basket frames are covered from all sides and insulated by glass wool from the inside and outside of the matrix. This was carried to prevent heat loss and to ensure that all the incoming air passes through the basket. One

side of the basket provided with an access door to remove or insert the matrices. Normally, all the baskets are filled with corrugated plate sheets. Other cases include porous layers of gravel and also the addition of metal by-pass tubes, where BR is the tubes facing area relative to the matrix facing area.

The schematic diagram of the testing rig is illustrated in figure (1), while the experimental arrangement is shown in figure (2). The test duct is provided by variable speed blower's at one side of the duct for supplying cold air to the matrix (as a discharge period mode) and the other side is to provide hot air to the matrix at the same time of charging period (as a charging period mode), A (40 kW) thermal capacity of the electrical heater system was placed at the entrance far away from the blower by 60 cm to provide the hot air. The heaters have 12 heating coils with a thermal capacity of 3.3 kW each, as shown in figure (3 A). The coils were distributed equally in a section, as shown in figure (3 B).

The hot duct is insulated with the glass wool material to stop the heating loss, while the cold duct was not. Three mixing baffles were placed on the duct after heaters as shown in figure (4), to ensure uniform temperature distribution of airflow in the hot duct. Moreover, Two layers of wire mesh (straightener) are provided to achieve a homogenous air velocity and it was is located before the entrance of the test section (15 cm between them), as shown in figure (5). The duct is supplied with four doors for a proper switching the periodic timing so that both the blowers are continually operating in each mode without interaction between them at the matrix where the doors were numbered in the schematic diagram as shown in figure (1). All the doors are provided with spring for quick response in shut off and opening when switching to another mode. The doors are sealed to prevent air leakages. The switching time

selected for change from the period mode to another mode is 90 sec. The matrix heating elements are divided into hot and cold plates.

The test rig matrix contains five baskets having an equal size for easy human handling due to the heavyweight of the plates, each basket is spaced from another one about 15 mm. According to the design listed in the table (1), the upper three and the lower two baskets are filled with hot and cold plates types, respectively. Five baskets in equal size have been filled with corrugated plates when a (P_{matrix}) matrix was tested. The modified matrix corrugated plates with coarse gravel ($P+CG$) was tested by changing the corrugated plates at the last cold plates basket (P_{matrix}) matrix with the gravel media and placed inside the cold end air preheater basket, as shown in figure (6). It was occupied about 20% in volume of the total matrix, and the basket filling with the heating elements is shown in figure (7). Figure (8) displays the top view of tubes inserted along with the matrix where the tube length is equal to the 0.9 m matrix length. The tube internal diameter is 19 mm while the thickness is 1.5 mm. The total by-pass tube facing area about 6% of facing area matrix. The by-pass tubes were arranged inside the gravel basket with the corrugated plate baskets to allow a controlled amount of flow to pass inside tubes that permeate the gravel and corrugated plate matrix. The operation procedure listed in the table (2)

Table (1): The rotary air preheater matrix in south Baghdad thermal power plant technical parameters [10].

Region	Plates material	Layer height (mm)	Plates Porosity (ϵ)	Material specific heat capacity (C_p)(J/Kg.K)
Hot end side	Carbon steel	500	0.84	465
Cold end side	Corten steel	350	0.77	460
Cold end side	gravel	150	0.41	840

Table (2): The test rig operations modes.

Mode type	Periodic time (sec)	Door opening (No.)	Door shut off (No.)
Charging mode (hot flow)	90	3 and 4	1 and 2
Discharging mode (cold flow)	90	1 and 2	3 and 4

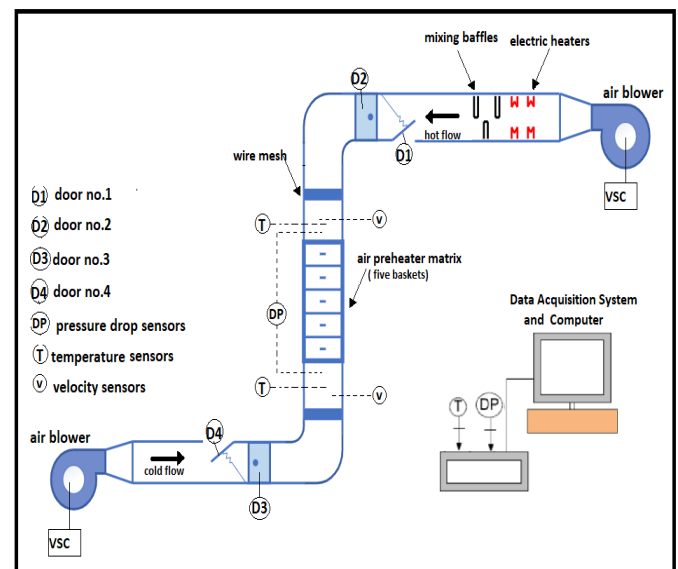


Figure 1. The schematic diagram of the test rig.



Figure 2. Experimental arrangement.

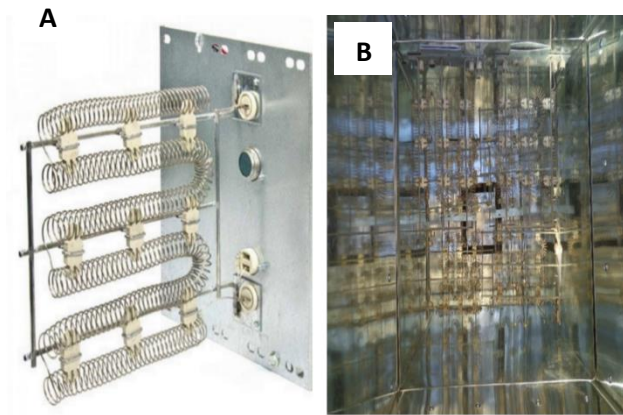


Figure 3. A-Electrical heater B- Distribution of heaters inside ducts.



Figure 4. Mixing Baffles



Figure 5. The Mesh Wire.



Figure 6. The gravel size of the matrix that has chosen.

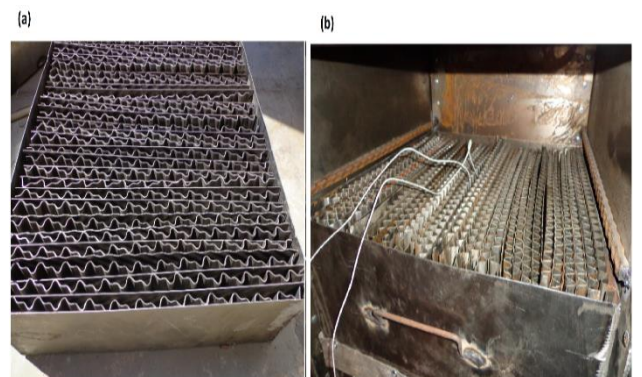


Figure 7. The corrugated plates profile filled inside the basket at (a) hot basket, (b) cold basket.

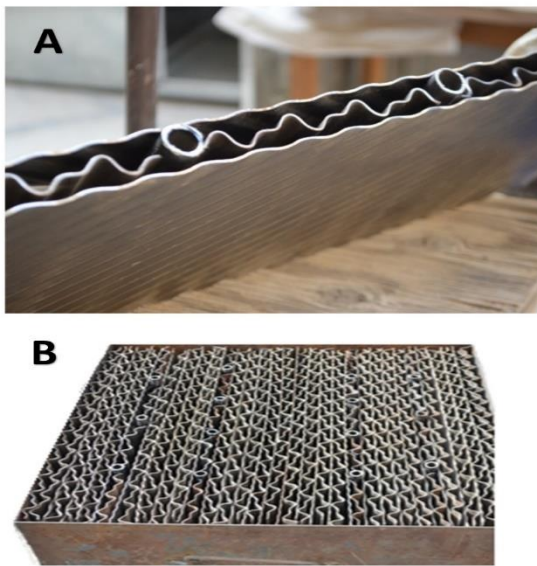


Figure 8. Geometry by-pass tubes distribution which is inserted between the corrugated **A**- Symbols **B**-by pass tube inside the basket.

3. Measuring Devices

Two data loggers (model: BTM-4208 SD) were employed. Each one contains twelve channels to record the temperature in an SD card with time, as shown in figure (9). Twenty-two thermocouple sensors have been used to measure and record both hot and cold temperature of metal and air for corrugated plate and gravel in the test section. The temperature recorder time intervals were taken every 10 seconds during the processes. The length of the thermocouples wires was 2 and 3 m and consisted of two wire legs. The wire's legs are welded together at one end creating a junction. The type of thermocouples is Type K (Nickel-Chromium /Nickel-Aluminium) with a temperature range of -50°C to 370°C . The accuracy of thermometer sensors was $(\pm 0.1^{\circ}\text{C})$. The thermocouples were fixed at different locations, the distribution inlet, outlet of the test section and between the baskets are given in figure (10) [11].

For checking the temperature profiles inside the cross-sectional plane of the duct, two-bracket frames were fixed between the wire-mesh and test section at the top and bottom of the test section. Seven thermocouples for each frame were fixed by wire in a horizontal plane on the

frame. The thermocouples sensor distribution on the frame was fixed and arranged, as shown in figure (11). The average and maximum temperatures were measured. The results concluded that the duct hot air temperatures at each point were nearly constant except a little increase in temperatures at the core of the duct by about 2°C among the others.



Figure 9. Digital data loggers.

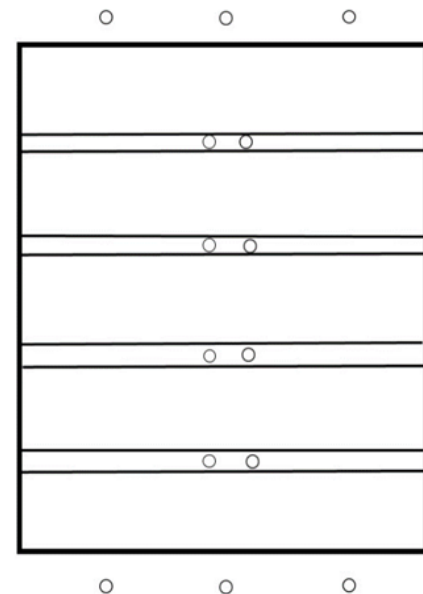


Figure 10. The side view position of thermocouples distribution in the test section.

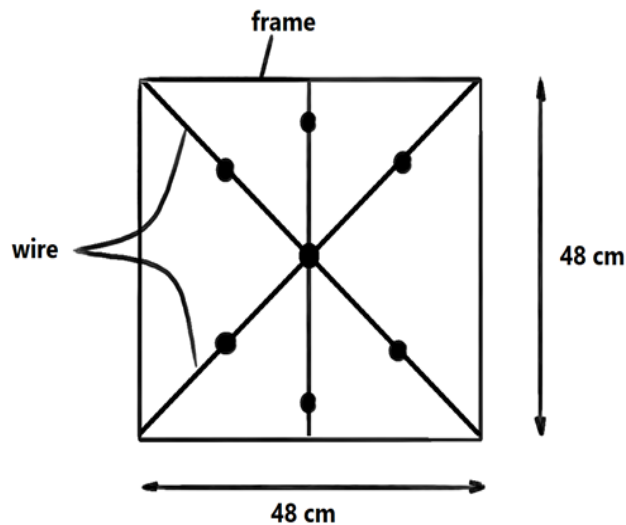


Figure 11. The thermocouples sensor distributed at the inlet and outlet test section.

The average air velocities were measured by a hot-wire anemometer (model AM-4214SD), as shown in figure (12), the percentage of errors did not exceed (0.0534 %).



Figure 12. The hot wire meter

The pressure drop across the test section was measured through digital pressure manometers, model (HT-1890 LCD Digital Gauge Differential Air pressure meter manometer) as shown in figure (13) with accuracy $\pm 0.55\%$.



Figure 13. Digital Pressure manometer.

4. The Test Procedures

The essential procedures for doing the experimental tests are illustrated as below:

- 1- Opening the door No.2 figure (1) to allow the surrounding cold air to pass through the matrix and ensure that the temperature of the domain is uniform.
- 2- Opening the door No.1 to charge hot air to the out, turn on both blowers and set the required flow rates, as the adjustment is discussed in previous sections. Measure the pressure drops and the averages velocity in cold airside. Turn on the switches of the heaters sequentially. After that, wait about 2 min to ensure that the charged hot air reaches steady-state conditions. The system now is ready for the test.
- 3- Press the recording in the data loggers and then quickly opening the door No. 4 and 3. Following that, closing door No. 2 and 1 sequentially for equipment safety. The hot air will be charged passing through the matrix and flow out from the door No. 3. The cold air should be still in flow leaving out from door No. 4. For the charging hot air, we need to wait to the end time the charging period.
- 4- After charging time is finished, quickly open the door No. 1 and 2 then close No. 3 and 4 sequentially. This will take the hot air charged out from door No.1 and the cold air passes to the matrixes lead to flow out at door

No.2. Wait then to complete the discharging period.

5- For the [(P+CG+T_s) and (P+CG+T_i) models], steps No. 2 and No. 3 are repeated six times aiming for achieving steady-state results in the transient temperature distributions of the matrix.

All the experiments were carried out in the cold and hot air temperatures ranged between 18 to 22.5 and 58 to 62.5 °C, respectively. To maintain stable hot air temperature at each specific flow rates, the heaters are switch on sequentially as flow rates increased.

5. The performance indicator for the air pre-heater

The air-preheater models in this study are a complex matrix containing different materials and different porosities of the heating elements. Besides that, the bypass tubes are embedded through the matrix. So, the simplest method to determine the performance of the different matrix models is by calculating the average heat transfer rates (Q_{av}) and the pumping power (PP) [12]. Since, the interesting thing for the air preheater performance is to increase the discharging outlet temperature, so all the equations were calculated during the discharging period as given in the following:

The heat transfer rate at a certain time (Q_t) is

$$Q_t = \dot{m} C_{p,a} (T_{in} - T_{out}) \quad (1)$$

In which

$$T_{in} = \sum(T_{in\ 1} + T_{in\ 2} + \dots + T_{in\ 7})/7 \quad (2)$$

And,

$$T_{out} = \sum(T_{out\ 1} + T_{out\ 2} + \dots + T_{out\ 7})/7 \quad (3)$$

Where, T_{in} and T_{out} are the average inlet and outlet air bulk temperatures of the duct, respectively at the discharging mode and the vice versa at the charging mode. The average air bulk temperature from equations 2 and 3 is calculated by the average of the seven points local temperatures at T_{in} and T_{out}

Thus, the average time heat transfer rate is

$$Q_{av} = \frac{1}{t} \int_0^t Q_t dt \quad (4)$$

The Reynolds number based on the duct hydraulic diameter is given by

$$Re = VD/\nu \quad (5)$$

In which V is the air average velocity in the duct, D is the hydraulic diameter of the duct. All of the thermo-physical properties of the air are determined at the overall bulk air temperature.

The pumping power is measured by the pressure drop across the matrix (ΔP) multiplied by the volumetric flow rate (\tilde{V}) is written as:

$$PP = \tilde{V} \Delta P \quad (6)$$

$$\text{In which } \tilde{V} = VA \quad (7)$$

Where: A is the duct cross-sectional area.

To assess the practical use of the enhanced matrix model, the performance is evaluated relatively by the average heat transfer rate dividing by pumping power in the form of thermal performance factor (η), which can be expressed as:

$$\eta = \frac{Q_{av}}{PP} \quad (8)$$

6. Results and Discussion

6.1 Pumping Power and the Heat Transfer Rate

The variation in pumping power along the different matrix models with the Reynolds number is shown in Figure (14). The pumping power in the (P+CG) model is higher than the other models due to that the low porosity of the gravel leads to increase the obstruction to flow and hence increase the pressure drop. The bypass tubes insertion is more effective for decreasing the pumping power, so more fluid flow passes through the smooth tubes without any obstruction. In the matrix (P+CG+T_i) model, the pressure drop is less the than

(P+CG+T_s) model, so more fluids pass on tubes without heat exchange. However, the (P_{matrix}) model is given less pressure drop.

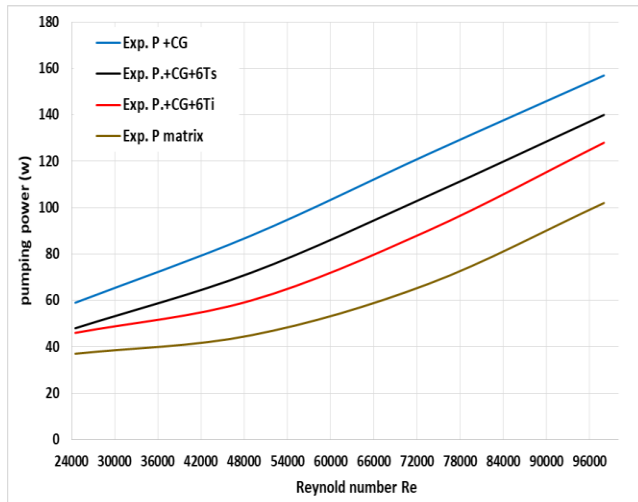


Figure 14. Variations of the pumping power with Reynolds number for different matrix models.

Figure (15) depicts the average heat transfer rate (Q_{av}) for different matrix models, as seen, there is no difference between (P_{matrix}) and (P+CG) models, so that the gravel media have no effect on the improved heat transfer to the matrix. The two models increased linearly with the Reynolds number. For other models, it shows that the bypass insertion (P+CG+T_i) and (P+CG+T_s) models have more signified for (Q_{av}) improved in (P+CG) model, but the (Q_{av}) increased slightly with Reynolds number when compared to previous models. This is because more amount of passing gases through the tubes without heat exchanged with the matrix as Reynolds number is increased. This issue gives a negative factor for the (Q_{av}) improvement rate for the inline model (P+CG+T_i) less than the staggered (P+CG+T_s) model, This confirms that the arrangement of tubes in this way is an important factor in improving heat transfer.

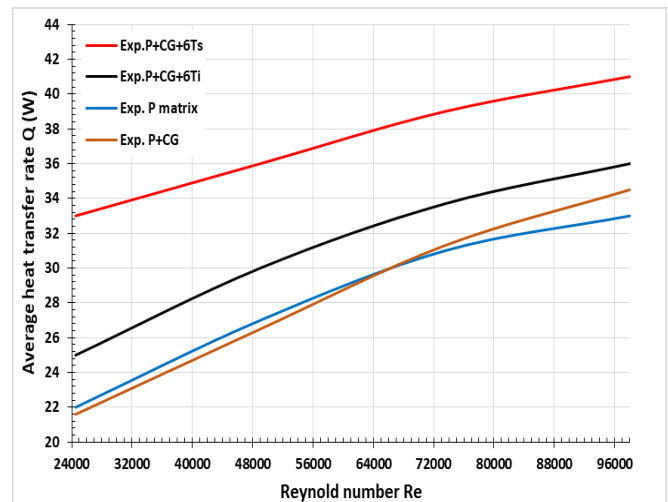


Figure 15. Variations of the average heat transfer rate with Reynolds number for different matrix models.

6.2 Thermal Performance factor

The variation of the thermal performance factor (η) with bypass tubes is depicted in figure (16). In this figure, the η tends to decrease with the Reynolds number. It is seen that the (P+CG+T_s) model gives the highest η along the range of Reynolds numbers and it shows the (P_{matrix}) model is higher than the (P+CG+T_s).

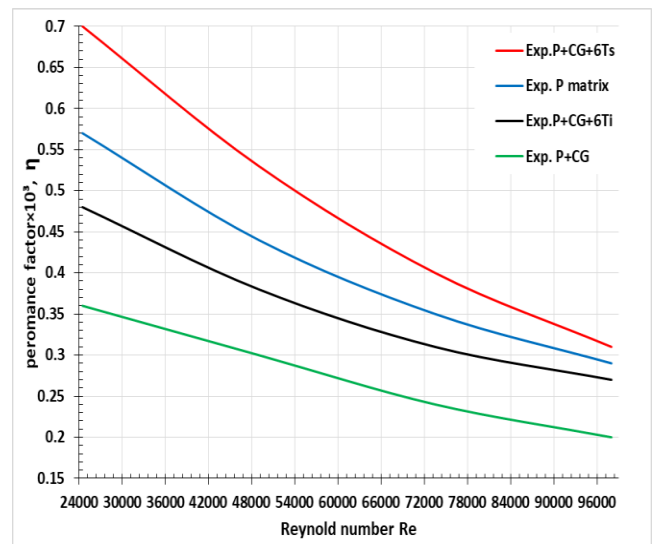


Figure 16. Variations of the performance factor with Reynolds number for different matrix models.

The outlet air temperature of the matrix for the models indicated that the (P+CG+T_s) model gives a higher outlet temperature during the

time as shown in figure (17).

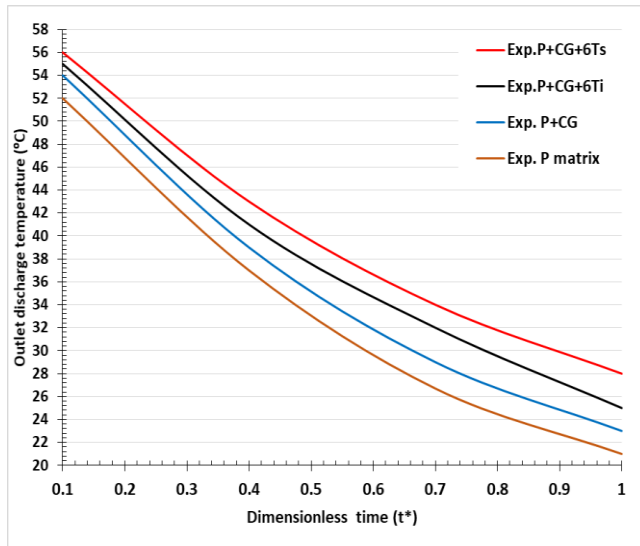


Figure 17. Variations of outlet discharge temperature with dimensionless time for different matrix models.

7. Conclusions

In this study, different models of air preheater matrix have been studied and compared with the standard air preheater matrix model, for proper change the last basket of the standard matrix to a corrosive resistance material in the modified matrix and to enhance the pressure drop and the heat transfer rates of the matrix by inserting a suitable ratio for bypass tube. The experimental work of a periodic-flow air preheater models have been studied to find the best performance factor. The following conclusions can be derived as :

- The (P+CG) model gives a high pressure drop and the same heat transfer rates as compared with the (P_{matrix}) model, which is that the average pumping power of the (P+CG) model is 23% higher than the (P_{matrix}) model.
- The bypass tubes give a significant improvement for the heat transfer rate (Q_{av}). The increased by 22% and 16% when compared to the (P_{matrix}) model with the (P+CG+T_s) and (P+CG+T_i) models, respectively.

- According to the range of Reynolds number the range of the performance factor (η) varies for the (P+CG+T_s) model from (0.7 to 0.31), meanwhile, for the (P_{matrix}) model, it varied from (0.57 to 0.29).for low to high Reynolds number, respectively.
- The temperature of the discharge outlet temperature for the (P+CG+T_s) model stays higher than other models during the discharging period, while the (P_{matrix}) model loses the energy before reaching the last time (0.75 t*)

8. Acknowledgements

The authors would like to thank the ministry of electricity (the state company of electrical production /middle region GCEP) and the collage of engineering / Mustansiriyah University, Baghdad, Iraq for their support to conduct this work.

9. Nomenclature

Q_{av}	Average heat transfer rate, w
Q_t	Heat transfer rate at a certain time, W
Re	Reynolds number
$C_{p,a}$	Specific heat capacity of air, kJ/ kg K
$C_{p,m}$	Specific heat capacity of the material, J/ kg K
BR	Relative bypass tubes facing area to the matrix facing area ratio% ,
T_{in}	Average inlet air bulk temperatures, °C
T_{out}	Average outlet air bulk temperatures, °C
D	Hydraulic diameter of the duct, m
v	Mean velocity in the duct, m /s
\dot{V}	volumetric air flow rate, m ³ /s.
PP	Pumping power, w
A	The duct cross-sectional area, mm ²
t*	Dimensionless time
η	Thermal performance factor, (= Q_{av}/ PP)

9.1 Greek letters

ν	Kinematic viscosity, m^2/s
ΔP	Pressure drop, Pa
ε	Porosity

9.2 Subscripts

$matrix$	Standard matrix model
av	Average

Conflict of interest

There are not conflicts to declare.

10. References

1. C. Alessandro, D. Giovanni, M. Giulio Di, M. Mirko, R. Franco, and S. Andrea, (2015): "A CFD-based virtual test-rig for rotating heat exchangers," *Energy Procedia* 82 245-251.
2. Akira Usami, Tadashi Noguchi, Hideshi Tezuka, Satoshi Nishimura and Takashi Kusunoki, (2003): "Development of a Water Dew Corrosion Resistant New Steel Element for Air Preheaters at Natural Gas Fired Power Plants." *Nippon Steel Technical Report* 87 10-13.
3. Shayan, M. R., Ranjbar K., Hajidavalloo E. and Heidari Kydan A. (2015) "On the failure analysis of an air preheater in a steam power plant," *Journal of Failure Analysis and Prevention* 15.6 941-951.
4. Ghodsipour, N., and M. Sadrameli, (2003) "Experimental and sensitivity analysis of a rotary air preheater for the flue gas heat recovery," *Applied Thermal Engineering* 23.5: 571-580.
5. Al-Kayiem, Hussain H., and H. A. A. Mahdi, (2010) "Performance enhancement of rotary air preheater by the use of pin-shaped turbulators," *Advanced Computational Methods and Experiments in Heat Transfer* XI 68:p.p:35.
6. Sreedhar Vulloju A., E. Manoj Kumar A., M. Suresh Kumar A and K. Krishna Reddy (2013): "Analysis of performance of Ljungstrom air preheater Elements," *Int. J. Curr. Eng. Technol* 2501-2505.
7. Heidari-Kaydan, A., and Hajidavalloo, E., (2014) "Three-dimensional simulation of rotary air preheater in steam power plant," *Applied Thermal Engineering* 73.1 :399-407.
8. Baba, K. V., MOHAN, P. P., and Kumar, T. J., (2016). "CFD Modelling And Simulation of 500MW Bisector Air preheater and Its Performance," *work* 3.11
9. Enlu Wang, Kai Li, Jinda Mao, Naveed Husnain, Deli Li and Wei Wu (2018) "Experimental study of flow and heat transfer in rotary air preheaters with honeycomb ceramics and metal corrugated plates," *Applied Thermal Engineering* 130 (2018): 1549-1557.
10. Buyukalaca, O. and T. Yilmaz, (2002) "Influence of Rotational Speed on Effectiveness of Rotary Type Heat Exchanger", *Heat and Mass Transfer*, Vol.38,.
11. Butrymowicz, D., Karwacki, J., Kwidziński, R., Śmierciew, K., Gagan, J., Przybyliński, T. and Łapin, M., (2016): "Methodology of heat transfer and flow resistance measurement for matrices of rotating regenerative heat exchangers." *Chemical and Process Engineering* 37.3 341-358.
12. Lee Young, Heeyoon Chung, Seon Ho Kim, Hyeng Sub Bae, and Hyung Hee Cho, (2017) "Optimization of the Heating Element in a Gas-Gas Heater Using an Integrated Analysis Model," *Energies* 10.12,P.1932.